



# Dissection of Conformational Conversion Events during Prion Amyloid Fibril Formation Using Hydrogen Exchange and Mass Spectrometry

Jogender Singh and Jayant B. Udgaonkar

National Centre for Biological Sciences, Tata Institute of Fundamental Research, Bangalore 560065, India

Correspondence to Jayant B. Udgaonkar: [jayant@ncbs.res.in](mailto:jayant@ncbs.res.in)  
<http://dx.doi.org/10.1016/j.jmb.2013.06.009>

Edited by R. Wetzel

## Abstract

A molecular understanding of prion diseases requires an understanding of the mechanism of amyloid fibril formation by the prion protein. In particular, it is necessary to define the sequence of the structural events describing the conformational conversion of monomeric PrP to aggregated PrP. In this study, the sequence of the structural events in the case of amyloid fibril formation by recombinant mouse prion protein at pH 7 has been characterized by hydrogen–deuterium exchange and mass spectrometry. The observation that fibrils are substantially more stable to hydrogen–deuterium exchange than is native monomer allows both forms to be quantified during the course of the aggregation reaction. Under the aggregation conditions utilized, native monomeric protein and amyloid fibrils are the only forms of the protein detectable during the course of the fibril formation reaction, suggesting that monomer directly adds on to the fibril template. Conformational conversion is shown to occur in two steps after the binding of monomer to fibril, with helix 1 unfolding only after helices 2 and 3 transform into  $\beta$ -sheet. Local stability in the  $\beta$ -sheet core region (residues ~159–225) of the fibrils is shown to be sequence dependent in that it varies along the length of the core, and local stability in protein molecules that are ordered in the structurally heterogeneous sequence segment 109–132 is shown to be similar to that in the core. This new understanding of the structural events during prion protein aggregation has important bearing on our comprehension of the molecular basis of prion pathogenesis.

© 2013 Elsevier Ltd. All rights reserved.

## Introduction

The autocatalytic conversion of the cellular prion protein, PrP<sup>C</sup>, into the misfolded and aggregated form, PrP<sup>Sc</sup>, is linked to several fatal neurodegenerative diseases [1,2]. While the structure of PrP<sup>C</sup> is known from NMR studies [3,4] to consist of an unstructured N-terminal domain (NTD) and a structured C-terminal domain (CTD) comprising three  $\alpha$ -helices and two short  $\beta$ -strands, that of PrP<sup>Sc</sup> is still poorly understood [2,5]. PrP<sup>Sc</sup> is known to be rich in  $\beta$ -sheet arranged in the characteristic structure of amyloid fibrils [6], but three different structural models suggest very different structures for PrP<sup>Sc</sup> (Ref. [5]). Understanding the mechanism of the conversion of PrP<sup>C</sup> into PrP<sup>Sc</sup>, in both kinetic and structural terms, is an important goal in prion biology, and structural characterization of the kinetic events during this conversion will lead to a better understanding of the molecular basis of the prion diseases.

*In vitro* studies of amyloid fibril formation by recombinant prion proteins provide a handle for understanding PrP<sup>C</sup>-to-PrP<sup>Sc</sup> conversion [5,7]. At physiological pH in the presence of denaturants, the prion protein can be made directly forming long straight, 8- to 10-nm-wide amyloid fibrils [8]. At low pH, it forms different types of  $\beta$ -rich oligomers under various conditions [8,9] that may further lead to the formation of worm-like fibrils [10–12]. Amyloid aggregates formed under various conditions have been shown to be cytotoxic [13,14], possibly because they can disrupt membrane structure [12]. Indeed, fibrils generated *in vitro* from recombinant PrP under different physicochemical conditions can be infectious [15,16]. Several experimental studies, including hydrogen–deuterium exchange (HDX) measurements [12,17,18], EPR [19], solid-state NMR [20], and solution NMR [21], show that the core region of the amyloid fibrils formed by different recombinant PrPs under different conditions are all

formed by the same sequence segment in the CTD of the protein. Nevertheless, the sequence dependence of local stability in the amyloid core formed under any aggregation condition by any of the prion proteins still needs to be delineated. HDX-mass spectrometry (MS) studies have emphasized the similarity of PrP<sup>Sc</sup> aggregates to aggregates of amyloid fibrils formed by recombinant prion protein [22,12].

It appears now that the core of amyloid fibrils formed by recombinant proteins is formed by the CTD adopting an in-register parallel  $\beta$ -sheet structure [19,20,12], but there is no experimental delineation of how this  $\beta$ -sheet in PrP<sup>Sc</sup> forms from the  $\alpha$ -helices in PrP<sup>C</sup>. Molecular dynamics simulations suggest different ways by which this conformational conversion might happen. One group of simulations suggests that the first step is the formation of a metastable monomeric state PrP<sup>C\*</sup>, in which helix 2 ( $\alpha$ 2) and helix 3 ( $\alpha$ 3) have undergone drastic structural changes [23,24]. Indeed, high-pressure NMR studies have identified a sparsely populated metastable conformation of PrP<sup>C</sup>, in which  $\alpha$ 2 and  $\alpha$ 3 are preferentially disordered [25]. On the other hand, other simulations carried out with shaPrP (109–219) at low pH suggest that conformational conversion involves structural rearrangements in the N-terminal region with  $\alpha$ 2 and  $\alpha$ 3 retaining their native conformations and helix 1 ( $\alpha$ 1) retaining its native conformation either partially [26] or completely [27]. Hence, the molecular dynamics simulations give conflicting results and bring out the necessity of carrying out experimental characterization of the conformational conversion reaction.

In the current study, the structural events occurring during the conversion of the full-length recombinant mouse prion protein (moPrP) to mature amyloid fibrils at pH 7 have been delineated temporally using HDX-MS. Firstly, it is shown that, unlike at low pH where oligomers are populated during the formation of worm-like fibrils [12], native monomeric protein and conformationally converted amyloid fibrils are the only detectable forms of the protein present at all times during the course of the aggregation reaction at pH 7. It is shown that local stability in the  $\beta$ -sheet core region mapping at residues ~159–225 in the mature amyloid fibrils of moPrP is sequence dependent along the length of the core. Finally, it is shown that the unfolding of  $\alpha$ 1 occurs after prior conformational conversion of  $\alpha$ 2 and  $\alpha$ 3 into more stable  $\beta$ -sheet.

## Results

In this study, HDX-MS has been used to characterize structurally the conversion of native monomeric mouse prion protein into amyloid fibrils at pH 7. Full-length recombinant moPrP has been used, and two different labeling pulses that were about 10-fold different in their labeling strength were used to probe structure. Since the intrinsic rate of HDX is 10-fold faster at pH 8 than at pH 7, the pH 8 pulse can label more strongly protected structure than can the pH 7 pulse. The use of strong pH 8 and weak pH 7 labeling pulses allowed the mechanism of the transformation of the  $\alpha$ -helices of monomeric moPrP into the  $\beta$ -sheet of amyloid fibrils to be studied.

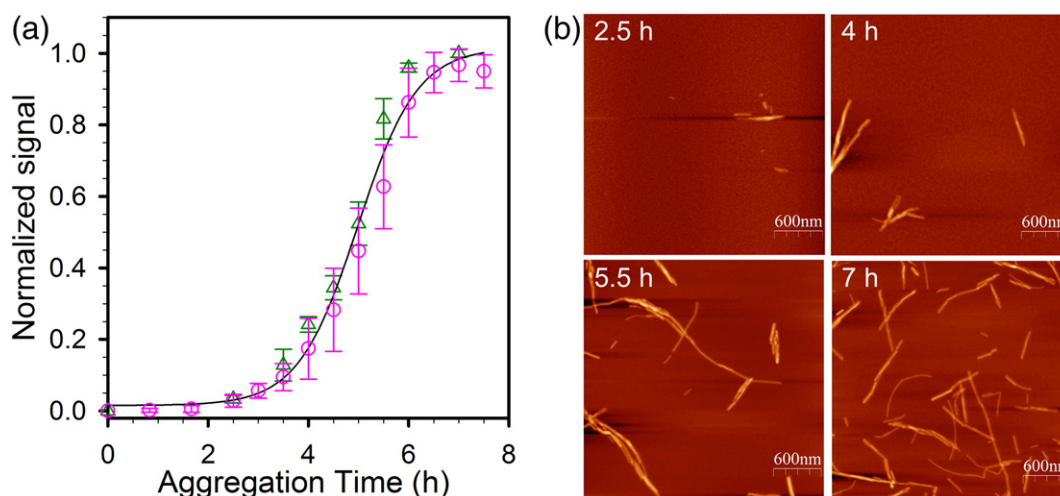


**Fig. 1.** Amyloid fibril formation by moPrP at pH 7. (a) Kinetics of fibril formation probed by ThT fluorescence measurements ( $\circ$ ) and fibril concentration measurements ( $\Delta$ ) using the sedimentation assay (see [Materials and Methods](#)) at different times of aggregation. The line through the data represents a fit to Eq. (1) and indicates that 50% of the aggregation reaction is complete at 5.20 h. (b) AFM images in topography mode of aggregating protein samples at different times of aggregation. The Z-height for all the images corresponds to 27 nm. The error bars in (a) represent the standard deviations from four independent experiments.

### Prion protein forms amyloid fibrils at pH 7

The prion protein is known to form long straight amyloid fibrils at pH 7, when agitated in the presence of denaturants and salts [8,17]. In the current study, moPrP aggregation was carried out at pH 7, 37 °C, in the presence of 1 M guanidine hydrochloride (GdnHCl), with agitation. Under this aggregation condition, moPrP aggregates with sigmoidal kinetics when monitored either by the thioflavin T (ThT) fluorescence assay or by a sedimentation assay (Fig. 1a). The formation of amyloid fibrils was confirmed by atomic force microscopy (AFM) (Fig. 1b), which reveals long straight fibrils similar in appearance and dimensions (8–10 nm diameter) to those observed in previous studies [8,28]. To visualize the aggregates formed during the course of aggregation of moPrP, aliquots of the aggregating protein were withdrawn at different times and studied using AFM. Only long straight amyloid fibrils are seen at different times of aggregation, and no oligomeric structures are seen during the course of aggregation (Fig. 1b). It should be noted that the fibrils stick strongly to mica surface, and hence, it is likely that, if oligomers were present, they too would have stuck to the mica surface, as do the oligomers found to form at low pH [11,12].

Aliquots of the aggregating protein were withdrawn at different times of aggregation and centrifuged at 24,000g for 15 min. Static light scattering measurements show that the weight-averaged mass of the protein remaining in the supernatant solution is the same as that of the native monomeric protein and does not change during the course of the aggregation reaction. The far-UV circular dichroism spectrum and the hydrodynamic radius measured by dynamic light scattering measurement of the protein remaining in the supernatant at any time during aggregation are identical with those of monomeric protein (Fig. S1). It is known that a centrifugal force of 24,000g does not sediment down oligomers of moPrP as large as 50mers [12]. Hence, the static and dynamic light scattering results indicate that oligomers smaller than 50mers are not populated significantly during the formation of long straight fibrils at pH 7, under the aggregation conditions utilized in this study.

### Monomer and fibrils are the only observable forms during fibril formation

Amyloid fibrils can be expected to afford different levels and extents of protection against HDX at amide sites, than does monomeric protein. Figure 2a shows that this is indeed so for the intact protein. A 180-s deuterium labeling pulse at pH 7 results in more amide sites becoming deuterated in the native monomeric protein before fibril formation than in fibrils fully formed at 6 h of aggregation. The mass of

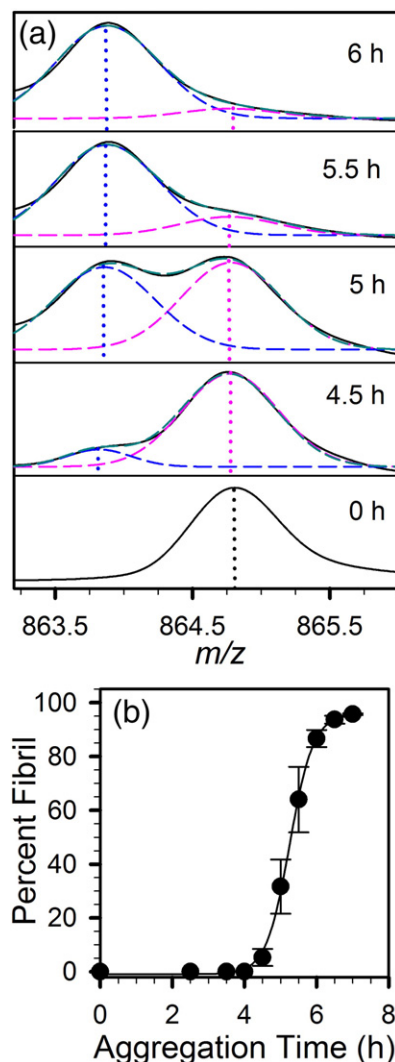


**Fig. 2.** Apparent two-state nature of the prion protein fibrillation. Aggregating protein was deuterated using a weak 180-s labeling pulse at pH 7. (a) Mass spectra of the +27th charge state of intact moPrP at different times of aggregation. The pink and blue broken lines represent the deconvoluted peaks, for monomer and fibrils, respectively. The dark-cyan broken line represents a fit to the sum of two Gaussian distributions, while the black line represents the raw data. (b) Percent fibril formation calculated from the area under the peak for fibril mass distribution relative to the total area under the peaks for both the monomer and fibril mass distributions. The line through the data indicates that 50% of the aggregation reaction is complete at 5.35 h. Error bars in (b) represent the standard deviations from three independent experiments.

the deuterium-labeled protein derived from monomer is found to be 25 Da more than deuterium-labeled protein derived from the fibrils. It should be noted that, for both monomer and fibrils, HDX was quenched by lowering the pH to 2.5 and that, in both cases, the protein was disaggregated/unfolded in

5.3 M GdnHCl and then desalted in exactly the same way before being fed into the mass spectrometer. When a strong 150-s labeling pulse at pH 8 is used instead of the weak 180-s labeling pulse at pH 7, the mass of deuterium-labeled protein derived from the fibrils does not change, but that of deuterium-labeled protein derived from monomer is found to be 37 Da more than deuterium-labeled protein derived from the fibrils (Fig. S2).

Since monomer and fibrils could be distinguished on the basis of the extent to which they underwent deuterium labeling, the kinetics of transformation of monomer into fibrils was studied by withdrawing an aliquot of aggregating protein at different times of

aggregation and subjecting the aliquot to HDX. Figure 2a shows that when the weak 180-s labeling pulse at pH 7 was used, only two forms of the protein are found to be labeled at different times of aggregation. One form is labeled to the same extent as is monomer, and another is labeled to the same extent as are fibrils. This indicates that monomer and fibrils are the only two forms of the protein present at all times of the aggregation process. If any other form were also present, either it would have to afford the same extent of protection as does either monomer or fibrils or it would have to be present to an undetectable extent. Figure 2b shows that the relative extent of fibrils increases in a sigmoidal

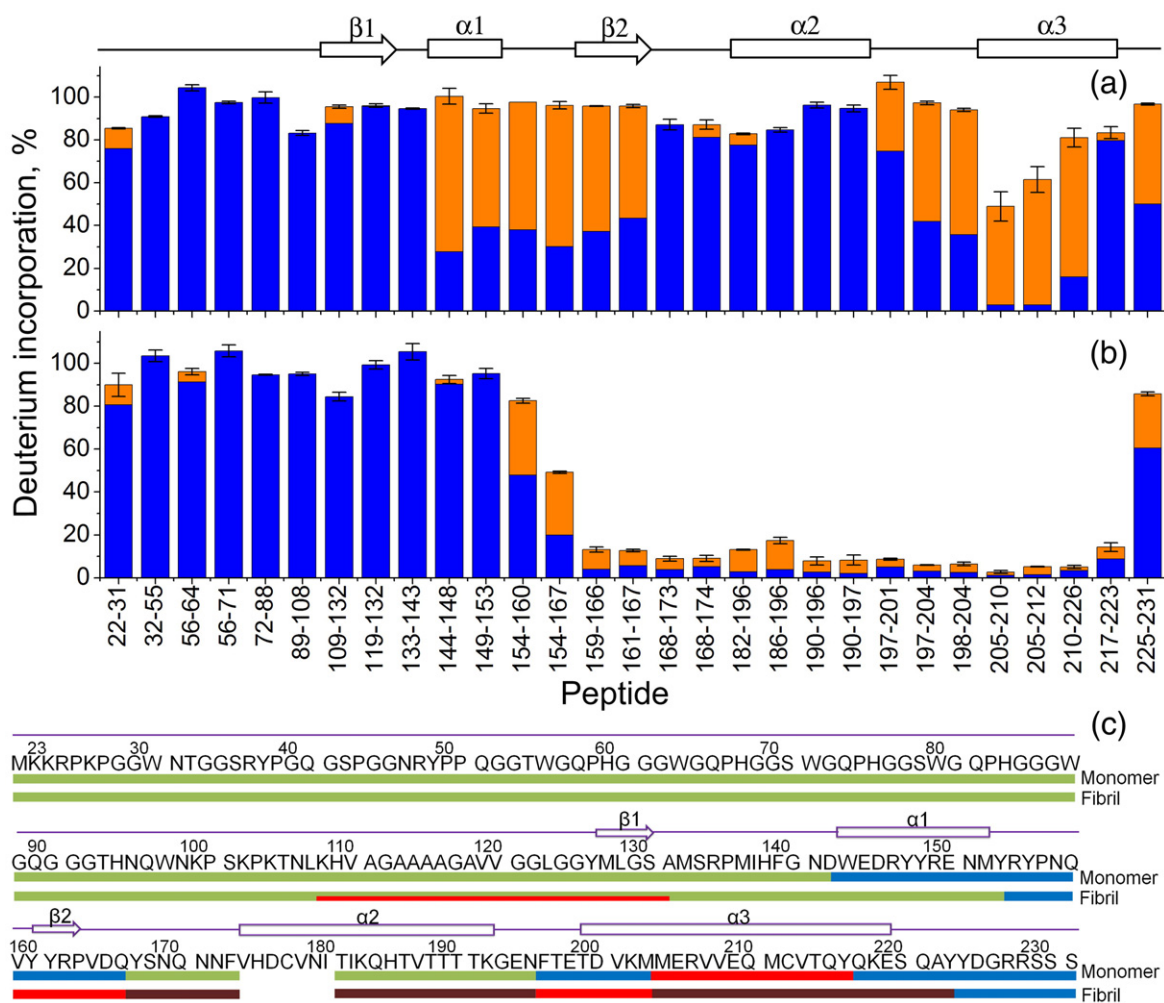


**Fig. 3.** Sequence segments in monomeric and fibrillar protein protected against HDX. The percent deuterium incorporation in different peptide segments of monomeric moPrP (a) and the final fibrils (b) is shown, for deuteration by the weak 180-s labeling pulse at pH 7 (blue bars) and by the strong 150-s labeling pulse at pH 8 (orange bars). The percent deuterium incorporation into each peptic fragment was determined as described in [Materials and Methods](#). Error bars represent the standard deviations from at least three independent experiments. (c) Sequence segments very strongly protected (protection factor,  $>10^5$ ), strongly protected (protection factor,  $10^4$ - $10^5$ ), moderately protected (protection factor,  $10^3$ - $10^4$ ), and weakly protected (protection factor,  $<10^3$ ) are shown as brown, red, blue, and green lines, respectively, below the protein sequence, for monomer as well as for fibril. Also shown as a half-green and half-red line is the sequence segment exhibiting conformational heterogeneity in the fibrils.

manner and that 50% of the protein has aggregated into fibrils at 5.35 h. Figure S2a and b shows that similar results are obtained when, instead, a strong 150-s labeling pulse at pH 8 is utilized.

#### Determination of the variation in local stability along the structural core of long straight amyloid fibrils formed by moPrP

The sequence segments in the fibrils formed at 7 h of aggregation at pH 7, which were deuterated by the labeling pulse (because of low protection against HDX), were identified by disaggregating the fibrillar protein immediately after labeling, desalting it, and then fragmenting it using pepsin digestion. On the basis of the peptide fragment map that has been generated earlier [12], MS was used to identify the peptide fragments that had undergone HDX and, hence, undergone an increase in mass, thereby identifying the sequence segments of the protein that are not protected against HDX in the aggregate. The same experiment carried out on native monomeric moPrP at pH 7, in exactly the same way as the experiment on the fibrils, identified the sequence segments that are protected against HDX in the native protein. Figure 3 shows the extents of labeling in monomer and in fibrils in different sequence segments of the protein. Figure 3a and b shows that the different segments, in the monomer as well as in the fibrils, are labeled either to the same extent or more, when the strong 150-s labeling pulse at pH 8 is used instead of the weak 180-s labeling pulse at pH 7. The former labels all sequence segments of the native protein nearly completely. Figure 3c shows the average protection factors for each sequence segment, in the monomer as well as in the fibrils, calculated from the data in Fig. 3a and b and mapped along the sequence of the protein. The protection factors were calculated by first determining the average intrinsic exchange rate for all the amides in a peptide fragment [29] and dividing this by the observed rate for that segment in the protein, which was determined by the extent of deuteration observed in the peptide fragment assuming an EX2 mechanism of exchange.

A comparison of the protection factors observed for the monomer and the fibrils (Fig. 3) reveals the following: (1) the sequence segment corresponding to  $\alpha 1$  is moderately protected in the monomer but weakly protected, if at all, in the fibrils; (2) the sequence segment corresponding to  $\alpha 2$  is weakly protected in the native monomer but strongly protected in the fibrils; (3) the sequence segment corresponding to  $\alpha 3$  is strongly protected in both monomer and even more so in the fibrils; (4) the sequence segment corresponding to  $\beta$ -strand 2 is moderately protected in the monomer but strongly protected in the fibrils; and (5) the core of the fibrils, defined as the sequence segments displaying strong

to very strong protection encompasses residues ~159–225.

#### Sequence segment 109–132 is strongly protected but in only 20% of the protein molecules in the fibrils

Significantly, sequence segment 109–132 shows a bimodal mass distribution in the fibrils, but a unimodal distribution in the native monomer (Fig. 4). This result indicates that this sequence segment of the protein in the fibrils exists in two different conformations, one that affords protection against HDX and the other one that affords only weak protection. This indicates that the protein molecules in the fibrils adopt two very

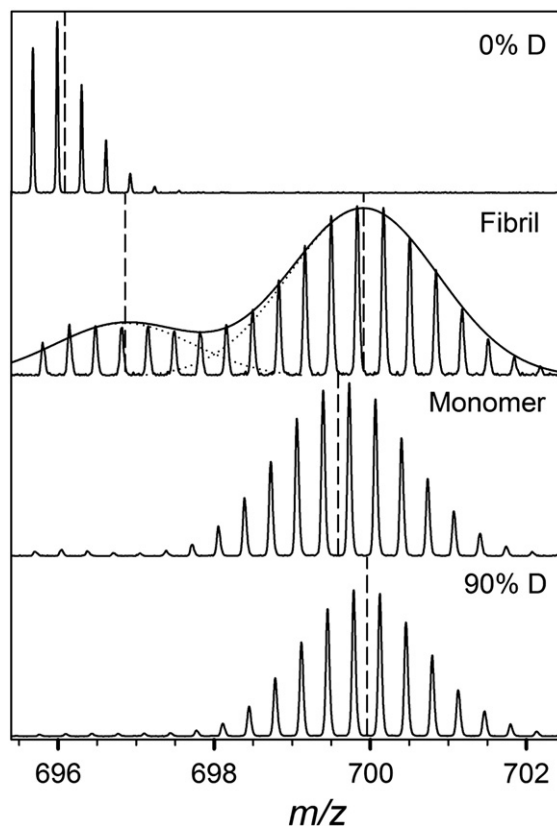


**Fig. 4.** Conformational heterogeneity in the amyloid fibrils. Mass spectra of peptide fragment 109–132 derived from monomer and from fibrils labeled by the weak 180-s labeling pulse at pH 7 are shown. Also shown are the mass spectra of protonated (0% D) and deuterated (90% D) peptides. The broken lines represent the average masses for the unimodal or bimodal mass distributions. The continuous line enveloping the bimodal mass distribution seen for the fibrils is a fit to the sum of two Gaussian distributions, with 20% of the total area being present under the lower mass distribution that is about 20% deuterated and 80% of the total area being present under the higher mass distribution that is 100% deuterated. Two individual peaks obtained from the fit to the sum of two Gaussian distributions are also shown as dotted lines.

different conformations for this segment of their structure. In ~80% of the protein molecules in fibrils, sequence segment 109–132 appears unstructured, while in the remaining ~20% of the fibril protein molecules, this sequence segment is sufficiently structured so as to afford strong protection against hydrogen exchange (Fig. 3).

### Monomer and fibrils are the only forms of moPrP detectable during fibril formation

HDX-MS experiments on the mixture of protein forms present at different times of aggregation indicate (Fig. 2) that monomer and fibrils are the only two forms of the protein present. To confirm that this is indeed so, aliquots of the aggregating protein solution were withdrawn at different times of aggregation, and subjected to centrifugation at 24,000*g* for 15 min. Upon HDX, the protein remaining in the

supernatant was found to have exactly the same quantitative pattern of protection, as does the monomeric protein at pH 7 (Fig. S3). The protein that sedimented down has exactly the same quantitative pattern of protection, as do the fibrils formed at 7 h of aggregation. There is no evidence for any conformation with a different quantitative pattern of protection.

### Sequence of conformational conversion events during the course of aggregation

Since the monomer and fibrils differ in both the extent of protection and the quantitative pattern of protection they afford to different segments of the protein, it was straightforward to examine how different segments of the protein change in these attributes during the course of amyloid fibril formation. Aliquots of the aggregating protein were withdrawn at different times of aggregation, sub-

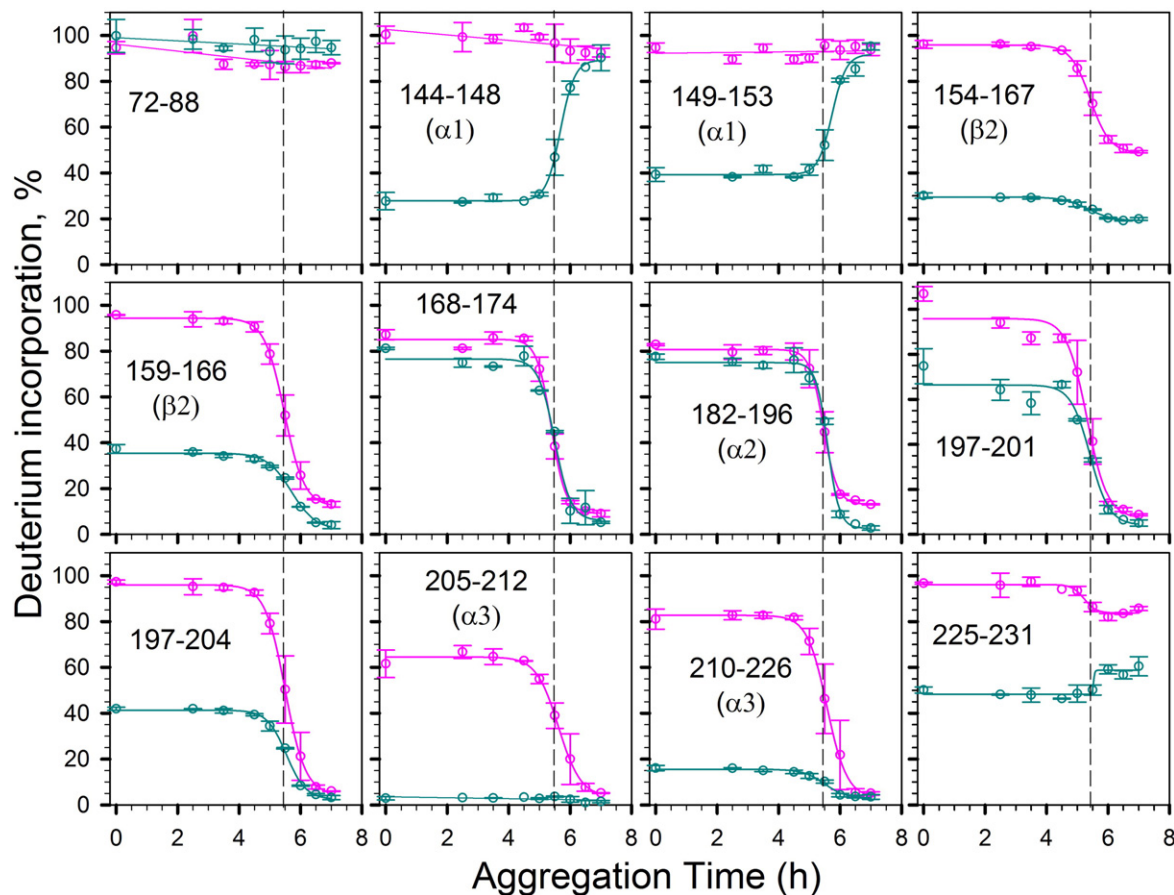


**Fig. 5.** Structural transformation in different secondary structure regions of moPrP. Percent deuterium incorporation profiles of representative peptide segments at different times of aggregation, obtained using a weak 180-s labeling pulse at pH 7 (dark cyan), as well as a strong 150-s labeling pulse at pH 8 (pink). The continuous lines drawn through all sigmoidal kinetic curves are fits to Eq. (1), and the sigmoidal kinetic curves for all sequence segments, except segments 144–148 and 149–153, have their midpoints ( $t_{50}$  values) at 5.46 h. The vertical broken lines across different plots are drawn at an aggregation time of 5.46 h as a guide to compare the  $t_{50}$  values of deuterium incorporation in different secondary structure regions. Different secondary structure regions are shown in bracket for different peptide segments. Error bars represent the spread in data from at least two independent experiments.

jected to HDX with either weak or strong labeling pulse, disaggregated using 5.3 M GdnHCl under HDX quenching conditions, and fragmented using pepsin digestion; the extent of deuteration in each fragment was determined by MS. The peptic fragments show bimodal mass distributions, with one peak corresponding to the monomer-derived fragment and other one corresponding to the fibril-derived fragment (Fig. S4).

Figure 5 shows the kinetic curves for deuterium incorporation in different sequence segments of protein in fibrils. These sequence segments correspond to different secondary structures in the native monomeric protein. The kinetic curves for all sequence segments (peptide fragments) are shown in Figs. S5 and S6. Both weak and strong deuterium labeling pulses were employed. The data reveal the following: (1) the sequence segment corresponding to  $\alpha 1$  in native monomer loses its protection completely with sigmoidal kinetics. The kinetics of the loss of protection is observable only with the weak labeling pulse because the strong labeling pulse labels this segment completely in the monomer itself (see above). (2) The level of protection afforded against HDX in the sequence segment corresponding to  $\alpha 2$  increases with sigmoidal kinetics. The decrease in the extent of deuterium incorporation as aggregation proceeds is seen when both the weak and strong labeling pulses were employed. (3) The sigmoidal increase in protection in the sequence segment corresponding to  $\alpha 3$  could be captured when only the strong labeling pulse was employed. The weak labeling pulse deuterated this sequence segment to the same extent at all times of aggregation. (4) The average  $t_{50}$  (the time at which a 50% change in deuterium labeling occurs) of structural rearrangement in the  $\alpha 1$  sequence segments 144–148 and 149–153, as probed by the weak labeling pulse, is  $5.71 \pm 0.03$  h. The  $t_{50}$  for all other secondary structure segments (mainly  $\alpha 2$  and  $\alpha 3$ ) is  $5.46 \pm 0.10$  h and is the same whether probed by the weak or the strong labeling pulse. Hence, the  $t_{50}$  of structural rearrangement in segment  $\alpha 1$  is different from that at segments  $\alpha 2$  and  $\alpha 3$ . It should be noted that although these  $t_{50}$  values differ to only a small extent, the difference is significant given that the measurements were performed simultaneously on the same protein molecules. The significance of the difference is reflected in the small errors in the measurements. (5) The observation that the  $t_{50}$  of structural rearrangement in any of the different sequence segments is the same whether the strong or the weak labeling pulses are used is expected if only monomer and fibrils are present during the course of aggregation. If an intermediate with intermediate protection against HDX were to be present, it would get labeled by the strong pulse but not by the weak pulse, and hence, the  $t_{50}$  values of structural rearrangements in different secondary

structure regions would have been different for the strong and weak labeling pulses.

## Discussion

The major goal of the current study, using HDX-MS, was to carry out a detailed structural characterization, secondary structure unit-wise, of how conformation conversion occurs during the course of conversion of monomeric mouse prion protein into mature amyloid fibrils at pH 7. A second goal was to determine whether protein forms other than monomer and mature fibril could be discerned at any time during the aggregation process at pH 7 and, in particular, whether oligomeric forms could be detected during long straight fibril formation at pH 7 as they have been for worm-like fibril formation at low pH [12]. A third goal was to determine whether local stability within the structural core of the fibrils, which was already known to reside in the CTD of the protein [12,17–21], varies along the length of the amyloid core and to determine whether and how local stability increases during the course of fibril formation.

### Local stability is sequence dependent in the fibril core formed in the CTD

The major obstacles in understanding the mechanism of prion pathogenesis are the lack of a structure for PrP<sup>Sc</sup> and the lack of an understanding of the structural events defining the conversion of PrP<sup>C</sup> into PrP<sup>Sc</sup>. Since high-resolution structural studies of brain-derived PrP<sup>Sc</sup> are not yet possible due to many practical problems [5], amyloid fibrils formed *in vitro* from recombinant PrP present themselves as a good practical proxy. Previous studies have shown that long straight fibrils formed by other prion proteins at pH 7 adopt a parallel in-register  $\beta$ -structure in the CTD of the protein [17–20,22]. It has also been shown previously that brain-derived PrP<sup>Sc</sup> may form  $\beta$ -strands either in the CTD [30] or in both the CTD and NTD (starting from residue ~89 or 90) [22]. In the current study, it has been shown that the core of the amyloid fibrils formed by moPrP resides in the CTD, specifically encompassing residues 159–225. Although it had been shown using different structural probes that the core region of PrP fibrils resides in the CTD, the boundaries of the core region had not been well defined. In the current study, unlike in previous studies, the definition of the structural core is based on quantitative determination of protection factors and, hence, local stability, along the sequence, and the core has been defined here as the sequence regions exhibiting strong to very strong protection against HDX (Fig. 3). The same quantitative determination of sequence-dependent local stability has

revealed that the N-terminal segment, as well as a middle segment of the amyloid core, is less stable than other region of the core (Fig. 3c). Interestingly, the CTD of PrP appears to adopt a parallel in-register  $\beta$ -structure even in the worm-like fibrils formed at low pH, as well as in the spherical oligomers on and off the pathway of worm-like fibril formation [9,12]. The observation that the same sequence segment forms the parallel in-register  $\beta$ -structure core in two very different types of fibrils formed under very different aggregation conditions led to an inspection of the amino acid composition of residue segment 159–225 of moPrP. It was found that 40% of the residues in this segment are F, I, V, T, N, and L, which are known to favor the formation of parallel  $\beta$ -sheets [31,32]. Only 14% of the protein sequence outside the core region is made up of these same six residues.

#### Local stability in the structurally heterogeneous segment 109–132 is either core-like or unstructured-like

Although the amyloid fibrils formed from recombinant PrP are infectious [15,16] and induce disease in healthy animals, their infectivity is found to be less than that of PrP<sup>Sc</sup> (Refs. [5] and [7]). This observation has called into question whether amyloid fibrils formed *in vitro* from recombinant protein are a good proxy for PrP<sup>Sc</sup>. The discovery that, at least, one region of the prion protein in fibrils can adopt multiple conformations (Fig. 4) suggests a reason why fibrils formed *in vitro* may not be as infectious as PrP<sup>Sc</sup>. If only one structural component in the fibrils formed *in vitro* is infectious and this component is a minor component, then the infectivity of the heterogeneous fibrils will appear to be less than that of PrP<sup>Sc</sup>. In this study, a variably structured region has been identified in sequence segment 109–132, and it is possible that the amyloid core extends down into the NTD in a small fraction of the amyloid fibril population. Indeed, the core of brain-derived PrP<sup>Sc</sup> also appears to extend into the NTD [22]. Importantly, in fibrils formed by the Y145 stop mutant variant of PrP, which is associated with a hereditary amyloid disease, the core region spans residues 109–132

[33,34]. Thus, this sequence segment seems to be important for the infectivity and the pathogenesis of the prion protein. Interestingly, the amyloid aggregates formed at low pH also show such conformational heterogeneity in this region [12], as do the amyloid fibrils generated by seeding with brain-derived PrP<sup>Sc</sup> (Ref. [18]). In the current study, it is seen that structure present in this segment has about the same local stability as does the structural core. In contrast, for both the worm-like fibrils formed at low pH [12] and the fibrils generated by seeding with brain-derived PrP<sup>Sc</sup> (Ref. [18]), the structure, when present in this sequence segment, is less stable than in the core region.

#### Fibril formation appears to be a two-state reaction

In several previous studies of long straight fibril formation by the prion protein, dimers and larger oligomers were observed to transiently accumulate [35–37]. In contrast, under the aggregation conditions utilized in the current study, monomer and fibrils are the only two forms of the protein that are detectable during the course of the reaction (Figs. 1 and 2), and no intermediate oligomers could be detected even with the use of multiple probes (see Results); hence, the aggregation reaction appears to be two-state. This suggests that when oligomer formation is observed under other aggregation conditions, it need not necessarily be a productive on-pathway event for fibril formation. Indeed, in the case of worm-like fibril formation by moPrP at low pH, one population of transient oligomers was shown to be off-pathway to the main fibril formation pathway [37]. Other proteins are also known to accumulate oligomers transiently under one aggregation condition and only monomer and fibrils under another aggregation condition [38].

If the fibril formation reaction of moPrP is indeed two-state in that monomer and fibrils are the only two forms present, it would imply that monomer adds directly to the fibril template and only then undergoes conformational conversion. Monomer addition followed by conformational conversion has also been reported for PrP seeds derived from infected hamster

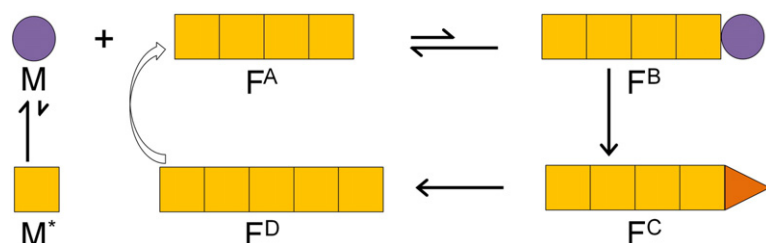


**Fig. 6.** Fibril growth via monomer addition and conformational conversion. In the scheme shown, conformational conversion occurs in two steps after monomer (M) addition to pre-existing fibril (F<sup>A</sup>). In the first step, F<sup>B</sup> to F<sup>C</sup>, the  $\beta$ -sheet core forms in region 159–225, and in the

second step, F<sup>C</sup> to F<sup>D</sup>, structure is lost in the  $\alpha$ 1 region. F<sup>D</sup> then becomes available for further monomer addition. The scheme also shows the conformationally converted M\*, which is too sparsely populated to be detected by HDX-MS and that is likely to be the source of the first fibrils that form. In this model, the formation of fibrils from M\* is likely to be very slow, compared to autocatalytic conversion of M on the fibril template. Hence, the bulk of fibril growth will occur by monomer addition directly to fibril.

brain [39–41] and also seems to be the case for fibril formation by the yeast prion protein Sup35NM [42]. In the case of Sup35NM aggregation, it was shown that monomer adds to the fibril one molecule at a time, but it has not been possible to demonstrate directly whether this is also true in the case of moPrP aggregation. Template-directed aggregation has been also observed for proteins such as tau [43], A $\beta_{1-40}$  [44], and  $\beta_2$ -microglobulin [45]. It should be noted that although the amyloid fibril formation reaction appears to be two-state in that monomer and fibrils are the only two observable forms, the conformational conversion of monomer newly added to the fibril template occurs in more than one step (Fig. 6).

### Mechanism of conformational conversion

The current study demonstrates, by showing that protection against HDX in residue segment 144–153 gets completely lost, that helix  $\alpha 1$  unfolds during the process of conformational conversion. By showing that protection against HDX in residue segments 182–196 and 197–226 increases significantly, this study suggests that helices  $\alpha 2$  and  $\alpha 3$  convert to more stable  $\beta$ -sheet structure. In general, protection factors for  $\beta$ -sheets are known to be higher than for  $\alpha$ -helices [46]. The increase in protection factors during the formation of the fibrils and the fact that prion protein fibrils formed under similar conditions have been shown to form parallel in-register  $\beta$ -sheet in the same core region [19,20] strongly suggest that the fibrils observed in the current study form a parallel in-register  $\beta$ -sheet. Importantly, it appears that conformational conversion in the  $\alpha 2$  and  $\alpha 3$  region of the bound monomer to  $\beta$ -sheet in the fibril is induced by the fibril template just before the unfolding of the  $\alpha 1$  region is induced (Fig. 6).

It has been suggested that PrP<sup>Sc</sup> and PrP<sup>C</sup> interact through  $\alpha 1$  and that the  $\beta 1$ - $\alpha 1$ - $\beta 2$  region is crucial for initiating the formation of the  $\beta$ -sheet amyloid core [2,47–49]. The observation made in this study that the structural transformation of  $\alpha 2$  and  $\alpha 3$  precedes that of  $\alpha 1$  indicates that this is not true for the amyloid fibrils studied here: conformational conversion initiates in sequence segment ~159–225, and not at  $\alpha 1$ . Indeed, it is known that the  $\alpha 1$  region is non-amyloidogenic and may delay, if not inhibit, the aggregation of PrP [50,51] and that a sheep PrP (167–227) fragment, corresponding to  $\alpha 2$  and  $\alpha 3$ , forms an amyloid structure similar to that of full-length PrP [28]. Moreover, in the course of worm-like fibril formation at low pH, only the oligomer in which  $\alpha 1$  has unfolded can form fibrils, while the oligomer that retains  $\alpha 1$  is unable to do so [12]. Computer simulation studies too indicate that conversion of PrP<sup>C</sup> into PrP<sup>Sc</sup> involves conversion of  $\alpha 2$  and  $\alpha 3$  into  $\beta$ -sheet [52,53]. The observation that initiation of prion protein aggregation occurs in segment 159–225 is consistent with studies showing

that several anti-prion drugs bind to this sequence segment, leading to the stabilization of PrP<sup>C</sup> (Refs. [54–56]). Locating more precisely the site in segment 159–225 where conformational conversion begins is important from the perspective of developing better therapeutics against prion diseases.

## Materials and Methods

### Protein expression and purification

Full-length moPrP (23–231) was expressed and purified as described previously [9]. It should be noted that the reverse-phase chromatography step is very critical for the aggregation kinetics at pH 7 to be reproducible. Before injecting into the reverse-phase chromatography column, the protein solution was diluted such that the absorbance peak at 280 nm was below 1.6 absorbance units, and protein was collected only until about 20% from the top, on the right side of the positively skewed protein peak.

### Buffers, solutions, and experimental conditions

All reagents used for experiments were of the highest purity grade available from Sigma, unless otherwise specified. The protein in 10 mM sodium acetate buffer (pH 4) was diluted 2-fold with 2 $\times$  aggregation buffer [100 mM Tris-HCl and 2 M GdnHCl (pH 7.45)] so that the protein was finally in 1 $\times$  aggregation buffer [50 mM Tris-HCl and 1 M GdnHCl (pH 7)]. To start the aggregation reaction, the protein in 1 $\times$  aggregation buffer was incubated at 37 °C and shaken at 750 rpm using an Eppendorf thermomixer. The final protein concentration used for all the experiments was 100  $\mu$ M. Sample handling and mixing were carried out very carefully so as to obtain reproducible aggregation kinetics.

### ThT fluorescence assay

ThT fluorescence was measured at pH 8.0 in 50 mM Tris-HCl buffer. A final concentration of 1  $\mu$ M protein and 10  $\mu$ M ThT was used. For every measurement, a calculated amount of protein was withdrawn from the aggregating protein solution and added into the ThT assay solution. Readings were taken within 20 s of the addition of protein into the ThT solution, using a Fluoromax-3 spectrofluorometer (Jobin Yvon) as described earlier [9].

### Sedimentation assay for fibril formation

Aliquots of aggregating protein were withdrawn at different times of aggregation and centrifuged at 24,000g for 15 min. The concentration of protein remaining in the supernatant was determined by measurement of absorbance at 280 nm using an extinction coefficient of 62,160 M<sup>-1</sup> cm<sup>-1</sup>. This yielded the amount of protein that sedimented down as fibrils.

### Atomic force microscopy

For AFM sample preparation, an aliquot of aggregating protein solution was withdrawn at pre-determined times,

diluted to 5  $\mu\text{M}$  in  $1 \times$  aggregation buffer, and then applied on to freshly cleaved mica (Grade V1; SPI Supplies). The sample was allowed to incubate for 1 min on the mica, rinsed with milli-Q water three times, and then dried under vacuum for 1 h. AFM images were obtained using a PicoPlus AFM instrument (Molecular Imaging, Inc.) operating in the non-contact mode using 75-kHz, 2.8-N/m cantilevers with a rounding tip radius of  $<10$  nm (Nano-World AG).

### HDX-MS measurements

The peptide map of moPrP was generated as described earlier [12]. To initiate deuterium labeling, a 20- $\mu\text{L}$  aliquot was withdrawn from the aggregation reaction and diluted into 180  $\mu\text{L}$  of aggregation buffer prepared in  $\text{D}_2\text{O}$  (pH 7.0 or 8.0 depending on the pulse strength, corrected for isotope effect) and incubated at 25  $^\circ\text{C}$ . At 180 s (pH 7) or 150 s (pH 8) of labeling, 200  $\mu\text{L}$  of the above sample was mixed with 400  $\mu\text{L}$  of ice-cold 8.0 M GdnHCl in 100 mM glycine buffer at pH 2.5 to dissolve the aggregate. After 2 min of incubation on ice, the samples were desalted using a Sephadex G-25 HiTrap desalting column equilibrated with water at pH 2.5 and an Akta Basic HPLC. The desalted samples were injected into the HDX module (Waters) coupled with a nanoAcquity UPLC for online pepsin digestion using an immobilized pepsin cartridge (Applied Biosystems). Further processing of the sample for mass determination using a Waters Synapt G2 mass spectrometer was carried out as described earlier [12]. For experiments involving the labeling of intact protein, the pepsin column and analytical column were removed, and the protein was eluted using a gradient of acetonitrile in a run of 4 min. The parameters used for the mass spectrometer measurements and the HDX module setup have been described earlier [12].

Peptide masses were calculated from the centroid of the isotopic envelope using the MassLynx software, and the shift in the mass of labeled peptide relative to the unlabeled peptide was used to determine the extent of deuterium incorporation at each time point of HDX. As the sample was in 90%  $\text{D}_2\text{O}$  during labeling and was exposed to  $\text{H}_2\text{O}$  after dissolution in GdnHCl, control experiments were carried out to correct for back-exchange and forward-exchange. To this end, moPrP was incubated in 10 mM sodium acetate (pH 4.0) (90%  $\text{D}_2\text{O}$ ) and fully deuterated by unfolding at 65  $^\circ\text{C}$  for 10 min followed by refolding on ice. Refolded moPrP was shown to be identical with native moPrP [12]. The fully deuterated moPrP sample was then processed in exactly the same way as the aggregates. Control experiments of labeling monomeric moPrP at pH 7 and pH 8 were also carried out in the same way as those of labeling the aggregated samples. The extent of deuterium incorporation in each peptide, % D, was determined using the equation % D =  $(m(t) - m(0\%))/(m(90\%) - m(0\%)) \times 100$ , where  $m(t)$  is the measured centroid mass of the peptide at time point  $t$ ,  $m(0\%)$  is the measured mass of an undeuterated reference sample, and  $m(90\%)$  is the measured mass of a fully deuterated reference sample (in 90%  $\text{D}_2\text{O}$ ) [57].

The percent deuterium incorporation for peptides showing a bimodal distribution was calculated as described earlier [12]. For calculation of the percent monomeric and fibrillar forms of intact protein at different times of aggregation, the bimodal mass distributions were

fit to the sum of two Gaussian distributions using OriginPro 8. The percentage of each form was calculated from the relative area under each peak.

### Data analysis and curve fitting

The kinetic curves measured by ThT fluorescence assay, percent fibril determined by HDX-MS of intact protein, and the percent deuterium incorporation for peptides in the different secondary structure regions of moPrP were fitted to the sigmoidal equation:

$$S = S_0 + \frac{S_\infty}{1 + e^{-((t-t_{50})/\tau)}} \quad (1)$$

where  $S_0$  is the signal at  $t = 0$ ,  $S_\infty$  is the amplitude of signal change,  $t$  is the time,  $t_{50}$  is the time at which the change in signal is 50%, and  $\tau$  is a characteristic time constant.

### Acknowledgements

We thank members of our laboratory for discussion and for their comments on the manuscript. The AFM images were collected at the Central Imaging Facility of the National Centre for Biological Sciences. J.B.U. is a recipient of a JC Bose National Fellowship from the Government of India. This work was funded by the Tata Institute of Fundamental Research and by the Department of Biotechnology, Government of India.

### Supplementary Data

Supplementary data to this article can be found online at <http://dx.doi.org/10.1016/j.jmb.2013.06.009>

Received 22 April 2013;

Received in revised form 10 June 2013;

Accepted 12 June 2013

Available online 25 June 2013

### Keywords:

prion;  
amyloid fibrils;  
mouse prion protein;  
hydrogen exchange;  
mass spectrometry

### Abbreviations used:

HDX, hydrogen–deuterium exchange; MS, mass spectrometry; NTD, N-terminal domain; CTD, C-terminal domain; AFM, atomic force microscopy; ThT, thioflavin T; GdnHCl, guanidine hydrochloride.

### References

- [1] Griffith JS. Self-replication and scrapie. *Nature* 1967;215: 1043–4.

- [2] Prusiner SB. Prions. *Proc Natl Acad Sci USA* 1998;95:13363–83.
- [3] Riek R, Hornemann S, Wider G, Glockshuber R, Wüthrich K. NMR characterization of the full-length recombinant murine prion protein, mPrP(23–231). *FEBS Lett* 1997;413:282–8.
- [4] Zahn R, Liu A, Lührs T, Riek R, von Schroetter C, López García F, et al. NMR solution structure of the human prion protein. *Proc Natl Acad Sci USA* 2000;97:145–50.
- [5] Diaz-Espinoza R, Soto C. High-resolution structure of infectious prion protein: the final frontier. *Nat Struct Mol Biol* 2012;19:370–7.
- [6] Pan K-M, Baldwin M, Nguyen J, Gasset M, Serban A, Groth D, et al. Conversion of  $\alpha$ -helices into  $\beta$ -sheets features in the formation of the scrapie prion proteins. *Proc Natl Acad Sci USA* 1993;90:10962–6.
- [7] Legname G, Baskakov IV, Nguyen HB, Riesner D, Cohen FE, DeArmond SJ, et al. Synthetic mammalian prions. *Science* 2004;305:673–6.
- [8] Baskakov IV, Legname G, Baldwin MA, Prusiner SB, Cohen FE. Pathway complexity of prion protein assembly into amyloid. *J Biol Chem* 2002;277:21140–8.
- [9] Jain S, Udgaonkar JB. Evidence for stepwise formation of amyloid fibrils by the mouse prion protein. *J Mol Biol* 2008;382:1228–41.
- [10] Jain S, Udgaonkar JB. Salt-induced modulation of the pathway of amyloid fibril formation by the mouse prion protein. *Biochemistry* 2010;49:7615–24.
- [11] Jain S, Udgaonkar JB. Defining the pathway of worm-like amyloid fibril formation by the mouse prion protein by delineation of the productive and unproductive oligomerization reactions. *Biochemistry* 2011;50:1153–61.
- [12] Singh J, Sabareesan AT, Mathew MK, Udgaonkar JB. Development of the structural core and of conformational heterogeneity during the conversion of oligomers of the mouse prion protein to worm like amyloid fibrils. *J Mol Biol* 2012;423:217–31.
- [13] Novitskaya V, Makarava N, Bellon A, Bocharova OV, Bronstein IB, Williamson RA, et al. Probing the conformation of the prion protein within a single amyloid fibril using a novel immunoconformational assay. *J Biol Chem* 2006;281:15536–45.
- [14] Simoneau S, Rezaei H, Sales N, Kaiser-Schulz G, Lefebvre-Roque M, Vidal C, et al. *In vitro* and *in vivo* neurotoxicity of prion protein oligomers. *PLoS Pathog* 2007;3:e125.
- [15] Kim JI, Cali I, Surewicz K, Kong Q, Raymond GJ, Atarashi R, et al. Mammalian prions generated from bacterially expressed prion protein in the absence of any mammalian cofactors. *J Biol Chem* 2010;285:14083–7.
- [16] Wang F, Wang X, Yuan CG, Ma J. Generating a prion with bacterially expressed recombinant prion protein. *Science* 2010;327:1132–5.
- [17] Lu X, Wintrodde PL, Surewicz WK.  $\beta$ -Sheet core of human prion protein amyloid fibrils as determined by hydrogen/deuterium exchange. *Proc Natl Acad Sci USA* 2007;104:1510–5.
- [18] Smimovas V, Kim J, Lu X, Atarashi R, Caughey B, Surewicz WK. Distinct structures of scrapie prion protein (PrP<sup>Sc</sup>)-seeded *versus* spontaneous recombinant prion protein fibrils revealed by hydrogen/deuterium exchange. *J Biol Chem* 2009;284:24233–41.
- [19] Cobb NJ, Sonnichsen FD, McHaourab H, Surewicz WK. Molecular architecture of human prion protein amyloid: a parallel, in-register  $\beta$ -structure. *Proc Natl Acad Sci USA* 2007;104:18946–51.
- [20] Tycko R, Savtchenko R, Ostapchenko VG, Makarava N, Baskakov IV. The  $\alpha$ -helical C-terminal domain of full-length recombinant PrP converts to an in-register parallel  $\beta$ -sheet structure in PrP fibrils: evidence from solid state nuclear magnetic resonance. *Biochemistry* 2010;49:9488–97.
- [21] Kumar J, Sreeramulu S, Schmidt TL, Richter C, Vonck J, Heckel A, et al. Prion protein amyloid formation involves structural rearrangements in the C-terminal domain. *ChemBioChem* 2010;11:1208–13.
- [22] Smimovas V, Baron GS, Offerdahl DK, Raymond GJ, Caughey B, Surewicz WK. Structural organization of brain-derived mammalian prions examined by hydrogen-deuterium exchange. *Nat Struct Mol Biol* 2011;18:504–6.
- [23] Dima RI, Thirumalai D. Exploring the propensities of helices in PrP<sup>C</sup> to form  $\beta$  sheet using NMR structures and sequence alignments. *Biophys J* 2002;83:1268–80.
- [24] Dima RI, Thirumalai D. Probing the instabilities in the dynamics of helical fragments from mouse PrP<sup>C</sup>. *Proc Natl Acad Sci USA* 2004;101:15335–40.
- [25] Kuwata K, Li H, Yamada H, Legname G, Prusiner SB, Akasaka K, et al. Locally disordered conformer of the hamster prion protein: a crucial intermediate to PrP<sup>Sc</sup>? *Biochemistry* 2002;41:12277–83.
- [26] Alonso DOV, DeArmond SJ, Cohen FE, Daggett V. Mapping the early steps in the pH-induced conformational conversion of the prion protein. *Proc Natl Acad Sci USA* 2001;98:2985–9.
- [27] DeMarco ML, Daggett V. From conversion to aggregation: protofibril formation of the prion protein. *Proc Natl Acad Sci USA* 2004;101:2293–8.
- [28] Adrover M, Pauwels K, Prigent S, de Chiara C, Xu Z, Chapuis C, et al. Prion fibrillization is mediated by a native structural element that comprises helices H2 and H3. *J Biol Chem* 2010;285:21004–12.
- [29] Bai Y, Milne JS, Mayne L, Englander SW. Primary structure effects on peptide group hydrogen exchange. *Proteins* 1993;17:75–86.
- [30] Gong B, Ramos A, Vázquez-Fernández E, Silva CJ, Alonso J, Liu Z, et al. Probing structural differences between PrP<sup>C</sup> and PrP<sup>Sc</sup> by surface nitration and acetylation: evidence of conformational change in the C-terminus. *Biochemistry* 2011;50:4963–72.
- [31] Merkel JS, Sturtevant JM, Regan L. Sidechain interactions in parallel  $\beta$  sheets: the energetics of cross-strand pairings. *Structure* 1999;7:1333–43.
- [32] Fooks HM, Martin AC, Woolfson DN, Sessions RB, Hutchinson EG. Amino acid pairing preferences in parallel  $\beta$ -sheets in proteins. *J Mol Biol* 2006;356:32–44.
- [33] Helmus JJ, Surewicz K, Nadaud PS, Surewicz WK, Jaroniec CP. Molecular conformation and dynamics of the Y145Stop variant of human prion protein in amyloid fibrils. *Proc Natl Acad Sci USA* 2008;105:6284–9.
- [34] Damo SM, Phillips AH, Young AL, Li S, Woods VL, Wemmer DE. Probing the conformation of a prion protein fibril with hydrogen exchange. *J Biol Chem* 2010;285:32303–11.
- [35] Jansen K, Schafer O, Birkmann E, Post K, Serban H, Prusiner SB, et al. Structural intermediates in the putative pathway from the cellular prion protein to the pathogenic form. *Biol Chem* 2001;382:683–91.
- [36] Stöhr J, Weinmann N, Wille H, Kaimann T, Nagel-Steger L, Birkmann E, et al. Mechanisms of prion protein assembly into amyloid. *Proc Natl Acad Sci USA* 2008;105:2409–14.
- [37] Jain S, Udgaonkar JB. Prion protein aggregation. *Curr Sci* 2011;101:1311–27.

- [38] Carulla N, Zhou M, Arimon M, Gairí M, Giralt E, Robinson CV, et al. Experimental characterization of disordered and ordered aggregates populated during the process of amyloid fibril formation. *Proc Natl Acad Sci USA* 2009;106:7828–33.
- [39] DebBurman SK, Raymond GJ, Caughey B, Lindquist S. Chaperone-supervised conversion of prion protein to its protease-resistant form. *Proc Natl Acad Sci USA* 1997;94:13938–43.
- [40] Horiuchi M, Caughey B. Specific binding of normal prion protein to the scrapie form via a localized domain initiates its conversion to the protease-resistant state. *EMBO J* 1999;18:3193–203.
- [41] Horiuchi M, Priola SA, Chabry J, Caughey B. Interactions between heterologous forms of prion protein: binding, inhibition of conversion, and species barriers. *Proc Natl Acad Sci USA* 2000;97:5836–41.
- [42] Collins SR, Douglass A, Vale RD, Weissman JS. Mechanism of prion propagation: amyloid growth occurs by monomer addition. *PLoS Biol* 2004;2:e321.
- [43] Frost B, Ollesch J, Wille H, Diamond MI. Conformational diversity of wild-type Tau fibrils specified by templated conformation change. *J Biol Chem* 2009;284:3546–51.
- [44] Petkova AT, Leapman RD, Guo Z, Yau WM, Mattson MP, Tycko R. Self-propagating, molecular-level polymorphism in Alzheimer's  $\beta$ -amyloid fibrils. *Science* 2005;307:262–5.
- [45] Yamaguchi K, Takahashi S, Kawai T, Naiki H, Goto Y. Seeding-dependent propagation and maturation of amyloid fibril conformation. *J Mol Biol* 2005;352:952–60.
- [46] Englander SW, Kallenbach NR. Hydrogen exchange and structural dynamics of proteins and nucleic acids. *Q Rev Biophys* 1983;16:521–655.
- [47] Heller J, Kolbert AC, Larsen R, Ernst M, Bekker T, Baldwin M, et al. Solid-state NMR studies of the prion protein H1 fragment. *Protein Sci* 1996;5:1655–61.
- [48] Wille H, Michelitsch MD, Guenebaut V, Supattapone S, Serban A, Cohen FE, et al. Structural studies of the scrapie prion protein by electron crystallography. *Proc Natl Acad Sci USA* 2002;99:3563–8.
- [49] Govaerts C, Wille H, Prusiner SB, Cohen FE. Evidence for assembly of prions with left-handed  $\beta$ -helices into trimers. *Proc Natl Acad Sci USA* 2004;101:8342–7.
- [50] Ziegler J, Sticht H, Marx U, Muller W, Rosch P, Schwarzinger S. CD and NMR studies of prion protein (PrP) helix 1: novel implications for its role in the PrP<sup>C</sup>  $\rightarrow$  PrP<sup>Sc</sup> conversion process. *J Biol Chem* 2003;278:50175–81.
- [51] Ziegler J, Viehrig C, Geimer S, Rosch P, Schwarzinger S. Putative aggregation initiation sites in prion protein. *FEBS Lett* 2006;580:2033–40.
- [52] Baillod P, Garrec J, Colombo MC, Tavernelli I, Rothlisberger U. Enhanced sampling molecular dynamics identifies PrP<sup>Sc</sup> structures harboring a C-terminal  $\beta$ -core. *Biochemistry* 2012;51:9891–9.
- [53] Chen J, Thirumalai D. Helices 2 and 3 are the initiation sites in the PrP<sup>C</sup>  $\rightarrow$  PrP<sup>Sc</sup> transition. *Biochemistry* 2013;52:310–9.
- [54] Kuwata K, Nishida N, Matsumoto T, Kamatari YO, Hosokawa-Muto J, Kodama K, et al. Hot spots in prion protein for pathogenic conversion. *Proc Natl Acad Sci USA* 2007;104:11921–6.
- [55] Nicoll AJ, Trevitt CR, Tattum MH, Risse E, Quarterman E, Ibarra AA, et al. Pharmacological chaperone for the structured domain of human prion protein. *Proc Natl Acad Sci USA* 2010;107:17610–5.
- [56] Kamatari YO, Hayano Y, Yamaguchi KI, Hosokawa-Muto J, Kuwata K. Characterizing antiprion compounds based on their binding properties to prion proteins: implications as medical chaperones. *Protein Sci* 2013;22:22–34.
- [57] Zhang Z, Smith DL. Determination of amide hydrogen exchange by mass spectrometry: a new tool for protein structure elucidation. *Protein Sci* 1993;2:522–31.